Minerals Engineering 52 (2013) 62–73

Contents lists available at SciVerse ScienceDirect

Minerals Engineering

journal homepage: www.elsevier.com/locate/mineng

Gangue–reagent interactions during acid leaching of uranium

B.J. Youlton [a,b,*], J.A. Kinnaird [b]

[a] SGS South Africa, 58 Melville St., Booysens, Johannesburg, South Africa
[b] Department of Geology, University of the Witwatersrand, Johannesburg, South Africa

ARTICLE INFO

Article history:
Available online 29 April 2013

Keywords:
Ore mineralogy
Leaching
Reaction kinetics
Hydrometallurgy

ABSTRACT

During the acid leaching of uranium, gangue–reagent interactions have both negative and positive consequences. Gangue dissolution increases reagent costs, and in some cases can prevent the economic acid leaching of an ore, but can also increase uranium mineral exposure and improve recoveries. Due to rapid dissolution kinetics, the acid consumption characteristics of the various carbonate species are readily predicted, however the same is not true of silicate gangue. Due to factors including slower leach rates, incongruent dissolution, parabolic kinetics, and surface area, pH and temperature dependence, the gangue acid consumption characteristics of silicate minerals are significantly more complex. A detailed mineralogical investigation and acid leach tests were conducted on sandstone-hosted uranium ore samples. The dissolution characteristics of the more common gangue phases were determined. The study demonstrated that gangue–reagent interactions can be predicted from mineralogical data, thus reducing technical risk during processing.

1. Introduction

Uranium ores are processed by either an acid or an alkali leach (Abhilash et al., 2009). Acid leaches are typically preferred to alkali methods, as they frequently offer more rapid dissolution kinetics and are able to leach more efficiently at coarser grinds (Lunt et al., 2007). Alkali leaches are used where the reactivity of the gangue prevents acid leaching (Merritt, 1971; Lunt et al., 2007). However, under certain conditions it may not be possible to process an ore by alkali leach, for example if gypsum is present (IAEA, 1980). Therefore the nature of the gangue mineralogy can prevent the economic leaching of U. It would therefore be desirable to better understand the factors that influence gangue acid consumption and develop a method of quantitatively predicting gangue acid consumption from mineralogical data.

The major advantage of being able to model gangue acid consumptions from mineralogy (rather than simply performing a leach test), is that a model can be used to generate data for a range of possible conditions, while separate leach tests would be necessary for each condition of interest. The availability of mineralogical data also makes it possible to identify other potential mineralogical problems, such as clays.

In addition to contributing to acid consumptions, the dissolution of gangue minerals can aid in the recovery of valuable metals (Lottering et al., 2008). As the gangue dissolves, so the proportion of the mineral of interest that is exposed to the leach liquor increases, resulting in improved recoveries.

The gangue–reagent interactions that occur during the acid leaching of U, were investigated in order to understand their effect on reagent consumption and U dissolution. Samples were obtained from two Karoo-aged U occurrences. One sample was obtained from a U prospect within the main Karoo basin (sample MKB1) and three others (samples RAO, OAO and MSO) were obtained from the Kayelekera mine in Malawi.

1.1. Gangue mineral dissolution

Due to the rapid dissolution of carbonates, these minerals are typically considered to consume their stoichiometrically equivalent amount of acid during U leaching (IAEA, 1980). The dissolution of silicate minerals is more complex than that of carbonates. Due to the complex nature of silicate dissolution, it has been suggested that the dissolution of these phases cannot be predicted (IAEA, 1980). However, large amounts of research have been performed on the acid dissolution characteristics of silicate minerals since 1980. Much of this research (for example Lowson et al., 2005) was aimed at understanding the behaviour of gangue minerals during acid mine drainage, however due to similarities in pH and acid type, the information is readily transferred to U leaching.

Several factors influence the dissolution characteristics of minerals. The following factors influence the rate of mineral dissolution: mineral composition, time, temperature, pH, surface area

* Corresponding author at: SGS South Africa, 58 Melville St., Booysens, Johannesburg, South Africa.
E-mail address: Brandon.JayYoulton@sgs.com (B.J. Youlton).

0892-6875/$ - see front matter © 2013 Elsevier Ltd. All rights reserved.
http://dx.doi.org/10.1016/j.mineng.2013.03.030

and incongruent dissolution (Ross, 1969; Brantley and Conrad, 2008; Lüttge and Arvidson, 2008; Brantley, 2008).

Since minerals dissolve at a finite rate, the extent of dissolution is a function of time. However, the rate of dissolution can also vary with time. Generally two stages are seen during dissolution, (1) an initial more rapid rate which gradually slows to (2) steady-state dissolution (Brandt et al., 2003 and Brantley, 2008). The U leach tests typically include the initial phase of rapid dissolution but, (depending on the constituent minerals and conditions of the leach, may not necessarily reach steady-state dissolution. This decay from an initially rapid rate to steady state conditions is typically referred to as parabolic kinetics (Brantley, 2008). However, in practice, the change in rate as a function of time is more readily modelled by an exponential decay function, than a parabola.

The rate of mineral dissolution is considered to vary with temperature according to the Arrhenius equation (Brantley and Conrad, 2008).

$$k = A\ \exp(-E_a RT) \quad (1)$$

where k is the rate constant at a given temperature, A is the pre-exponential factor, E_a is the activation energy, R is the ideal gas constant and T is the absolute temperature (Brantley and Conrad, 2008). Using the Arrhenius equation it is possible to adapt kinetic data collected at one temperature to a more desirable temperature (Brandt et al., 2003).

Dissolution rates are typically normalised to the surface area of the mineral (Lüttge and Arvidson, 2008). Many workers (including Lowson et al. (2005); Brandt et al. (2003); Knauss and Wolery (1989)) favour the BET (Brunauer et al., 1938) method of surface area determination. This method allows for surface area determination by measuring the adsorption of an inert gas onto the surface of the sample. However, this is not as readily adapted to complex samples consisting of several minerals in various concentrations, such as is typically the case with U ores.

In addition to temperature and mineral surface area dependence, the release rate of an element from a dissolving mineral is influence by incongruent dissolution. Incongruent dissolution describes the case where elemental release rates are not proportional to the stoichiometry of the mineral (Brantley, 2008).

1.2. Reagents used in uranium leaching

Sulphuric acid is typically used to achieve the low pH required for acid U leaching (Ho and Quan, 2007). This acid has two acidic protons. The dissociation of the first proton has a sufficiently high equilibrium constant that it can be considered to proceed to completion, while the second dissociation has an equilibrium constant of 1.2×10^{-2} (Brown et al., 2003).

During acid leaching hexavalent U minerals tend to dissolve readily, while tetravalent U minerals require oxidation to the hexavalent state prior to dissolution (Lunt et al., 2007). In the processing of the Witwatersrand ores of South Africa, MnO_2 in the form of pyrolusite, is the preferred oxidant (Lottering et al., 2008). At Olympic Dam sodium chlorate is used (Miki and Nicol, 2009). Other oxidants include SO_2/O_2 (Ho and Quan, 2007), hydrogen peroxide and oxygen (Venter and Boylett, 2009). In this study only MnO_2 was considered. It has been found that these oxidising agents do not act on the U minerals directly, but instead serve to oxidise iron to the Fe^{3+} state, which in turn oxidises the U according to Eq. (2) (Lottering et al., 2008). This equation shows that the dissolution of MnO_2 consumes two moles of sulphuric acid for each mole of MnO_2 dissolved.

$$2Fe^{2+} + MnO_2 + 4H^+ \rightarrow 2Fe^{3+} + Mn^{2+} + 2H_2O \quad (2)$$

2. Methodology

In order to understand the response of the gangue minerals during leaching, the head samples underwent detailed mineralogical characterisation prior to acid leaching.

2.1. Gangue mineral characterisation

The samples were milled to the desired grind using a laboratory scale rod mill. All of the samples were milled to a P_{80} of 212 μm. Due to the large amount of MKB1 material, a second aliquot of this sample was milled to −75 μm and treated as a separate sample for the textural analyses and leach tests.

Both the head and leach residue samples were analysed by XRD and QEMScan bulk mineralogical analysis (BMA), to identify and quantify the gangue minerals present, and determine the mean grain size and degree of exposure of each gangue phase.

The XRD analyses were performed using the guidelines of McCusker et al. (1999). The powder samples were micronised and then analysed using a Panalytical X'pert Pro diffractometer and Co Kα radiation. The resulting data was processed using HighScore Plus software and the PanICSD database. Rietveld refinement was used to determine the quantities of each gangue phase.

QEMScan BMA analyses, conducted according the methods described by Gottlieb et al. (2000) and Coetzee et al. (2011), were also used in the gangue mineral quantification. The BMA analyses were performed on transverse cut polished sections, using a QEMScan based on a Carl Zeiss Evo 50 scanning electron microscope with four SiLi EDX detectors. The BMA and XRD data were validated against each other and against major element XRF data. In addition to XRF analyses, the samples were also analysed by titration to determine their Fe^{2+} content.

The BMA data was also used to determine the textural characteristics of the gangue. BMA analyses are more rapid and cost effective than other QEMScan techniques and therefore more readily applied to variability studies. For this reason the BMA was chosen over particle map analysis (PMA). However, BMA analyses are more prone to stereological bias than two dimensional scans, such as PMA (Sutherland et al., 1988), and it was necessary to stereologically correct the grain size data.

2.2. Uranium mineral characterisation

The U mineral characterisation was performed by QEMScan trace mineral search (TMS) using the same instruments used for the BMA analyses. The mineral identification was validated by manual scanning electron microscopy with associated energy dispersive X-ray analysis.

2.3. Leach tests

The batch acid leach tests were conducted using the guidelines given by the IAEA (1980 and 1990). Approximately 2 kg split aliquots of each sample were used. Due to the large amount of MKB1 material, it was possible to leach this sample at a number of different pH and Eh conditions and at two different grinds (P_{80} 212 and 75 μm). The limited amount of material in the Kayelekera samples limited these leach tests to one test per sample (P_{80} 212 μm).

The leaches were performed at a solid to liquid ratio of 1:1, in 5 L plastic beakers. Agitation was achieved by overhead stirrers. Temperature was controlled to between 35 and 40 °C. The pH was controlled using concentrated sulphuric acid and the redox potential was controlled using MnO_2, both Associated Chemical Enterprises, Platinum Line, analytical reagent grade.

A one hour preconditioning period was used. During this time the pH was controlled, but no attempt was made to maintain the redox potential (IAEA, 1990). After one hour of preconditioning the MnO_2 was added and this was considered to mark the beginning of the leach.

Slurry samples were taken after 1, 3, 8 and 24 h. These were filtered and the solutions submitted for U and Th by ICP-MS and Na, K, Al, Mg, Fe and Si by ICP-OES. The solids were rinsed with dilute sulphuric acid (pH 1.5). All of the residues were analysed by XRD and the 3 and 24 h samples were submitted for U and Th analysis by pressed pellet XRF and major elements by XRF borate fusion.

3. Modelling of gangue dissolution and reagent consumption

Based on the results of the XRD analyses and the ICP-OES analyses of the pregnant leach solution (PLS), the rates of decay of the various mineral phases were determined. In general the ICP-OES results were favoured over the XRD data due to their greater precision. However, in the cases of minerals which did not contain unique elements, it was necessary to use the XRD data. Fortunately these minerals were characterised by rapid dissolution and for this reason the error in the XRD data was small when compared to the decrease in concentration in each time interval.

In general the rates were modelled on the leach tests of the MKB1 sample and then tested against the Kayelekera samples. However, this was not possible for smectite and illite, which do not occur in the MKB1 sample.

3.1. Dissolution rates

An exponential decay function was used to account for the decrease in the rate of dissolution of the various mineral phases with time (Eq. (3)). Eq. (3) was adapted from an equation used in radioactive decay. This equation is given by Serway and Faughn (2003).

$$R = R_0 e^{(-\lambda t)} + z \tag{3}$$

where R is the rate at a given time (t), R_0 is the initial rate, λ is the decay constant and z is an approximation of the steady state dissolution rate. In practice the initial rate was usually so much more rapid than the steady state rate that, for most minerals, it was a reasonable approximation to set the steady state rate as zero. However, for leaches with a duration significantly longer than 24 h, it may be necessary to use a more precise treatment of the steady state condition.

Where this approximation was not valid, it was necessary to develop a function to predict the steady state rate. The relationship between pH and the steady state dissolution of many minerals is approximately parabolic (at least at the low pH used in acid U leaching), for example Lowson et al. (2005) with chlorite, and Kohler et al. (2003) for illite. Based on these results, parabolic functions were developed for the determination of z. In the same way, parabolic functions were developed to calculate R_0 from the pH of the leach test. The value of the decay constant was determined from the dissolution data. Again, a parabolic function was used to relate the value of the decay constant to the pH.

Taking the definite integral of Eq. (3) with respect to time (T) from 0 to t hours gives Eq. (4).

$$\int_0^t R\, dT = R_0 \frac{e^{-\lambda t} - 1}{-\lambda} + zt \tag{4}$$

Because most rates are surface area normalised, multiplying Eq. (4) by the surface area gives the percentage dissolution of the mineral. For example, if a mineral occurs in the ore in a concentration of 10%, and Eq. (4) gives 20% dissolution, then the concentration of the mineral in the leach residue would be 8% (ignoring the effect of the minerals dissolution on the total mass of the solids).

3.2. Surface area

Due to the complex mineralogy of the samples, geometric surface areas were chosen over the BET method. For most minerals a spherical model was applied, where the stereologically corrected mean grain size (from the QEMScan data) was used to estimate the surface area of the sample, according to Eq. (5) (modified from Tester et al., 1994).

$$A_{geo} = 6/\Phi_\rho \tag{5}$$

where A_{geo} is the specific geometric surface area (in m^2/g), Φ is the particle diameter (in μm) and ρ is the density of the mineral (in g/cm^3).

The spherical assumption was considered too simple to reliably model the phyllosilicates. Based on the work of Hodson (2006), the phyllosilicates were modelled as cuboids with equal lengths and breadths. Hudson used a 2 μm thickness for smaller grains and 4 μm for larger grains. In this study the thickness was taken as a linear function of the grain size, rather than using the Hudson's two classes. Hudson ignored the basal surface areas of the grains, while the entire phyllosilicate surface area was considered in the present study. This was done to maintain the similarity with BET surface areas.

The surface areas calculated using either Tester et al. (1994) or Hodson (2006) method tend to under estimate the true surface area of the mineral as they do not consider the effect of fractures and other surface roughness. This surface roughness can be calculated using Eq. (6) (Helgeson et al., 1984).

$$R_s = A_{ads}/A_{geo} \tag{6}$$

where R_s is the surface roughness, A_{ads} is the BET surface area and A_{geo} is the geometric surface area.

Using published dissolution studies that included both grain size and BET surface area data, the surface roughness of each mineral was calculated. It was found, based on the published data, that the roughness of many minerals is a function of the grain size. Therefore based on the data from several studies, linear relationships between grain size and surface roughness were established. Such detailed surface area data was not available for zeolite and so a simple geometric surface area was used for laumontite.

Because the QEMScan does not readily distinguish grain boundaries of very fine adjacent grains of the same mineral, it was not possible to determine surface areas for illite and smectite. A surface area of 42 m^2/g was used for illite (Bibi et al., 2011). No attempt was made to estimate the surface area of smectite because, the relationship between total surface areas and reactive surface areas are too complex to allow for surface area normalisation of smectite (Metz et al., 2005).

3.3. Mineral dissolution and acid consumption

The amount of acid consumed in the dissolution of a mineral depends on the composition of the mineral. Eqs. (7)–(15) show the acid dissolution of selected minerals. Calcite follows Eq. (7) (Venter and Boylett, 2009), laumontite follows Eq. (8), chlorite Eq. (9) (modified from Lowson et al. (2005) to more closely match the composition of the chlorite in the present study), muscovite is shown in Eq. (10) (Knauss and Wolery, 1989 and Oelkers et al., 2008), smectite is shown in Eq. (11), adapted from Amram and Ganor (2005) and Metz et al. (2005), illite in Eq. (12) after Kohler et al. (2003), plagioclase Eq. (13), K-feldspar Eq. (14) (both after Stillings and Brantley (1995)), quartz is shown in Eq. (15) (Blum et al.,

1990). As can be seen from Eq. (15), the dissolution of quartz does not consume acid. For this reason quartz will not be considered further.

Table 1
Acid consumption characteristics of selected minerals and MnO_2.

Mineral	Ideal acid cons (kg/ton)[a]	Incongruent acid cons (kg/ton)[a]
Calcite	9.8	–
Laumontite	6.4	3.8[c]
Chlorite	12.0[b]	–
Muscovite	12.3	–
Smectite	11.1[b]	–
Illite	10.7	–
Plagioclase	7.5[b]	6.1[c]
K-feldspar	6.8	2.7[c]
MnO_2	2.3	–

[a] Calculated using Eqs. (7)–(15), assuming 1% dissolution of the mineral of interest. When multiplied by the amount of the mineral that dissolved during the leach tests, these values can be used to calculate the acid consumed by each phase.
[b] These values vary with mineral composition.
[c] These values are strongly dependant on the element used to calculate the dissolution rate of the mineral.

Table 2
Major mineralogy as determined by XRD and QEMScan BMA.

Sample	MKB1 (Mass%)	RAO (Mass%)	OAO (Mass%)	MSO (Mass%)
Quartz	32.0	31.0	49.8	7.6
Plagioclase	25.5	40.7	40.1	16.6
K-feldspar	13.6	9.4	5.7	7.9
Muscovite	2.1	0.5	0.9	–
Chlorite	6.8	8.7	–	–
Illite	–	–	–	48.7
Smectite	–	8.2	3.4	19.2
Laumontite	8.1	–	–	–
Calcite	12.0	–	–	–
Pyrite	–	1.6	–	–
Total	100.0	100.0	100.0	100.0

$$CaCO_3 + 2H^+ \rightarrow CaSO_4 + CO_2 \uparrow + H_2O \quad (7)$$

$$CaAl_2Si_4O_{12}.4H_2O + 8H^+ \rightarrow Ca^{2+} + 2Al^{3+} + 4H_4SiO_4 \quad (8)$$

$$(Mg_{3.75}Fe_{6.25}Al_2)(Si_6Al_2O_{20})(OH)_{16} + 32H^+ \rightarrow 75Mg^{2+} + 6.25Fe^{2+} + 4Al^{3+}6H_4SiO_4 + 12H_2O \quad (9)$$

$$KAl_2(Si_3AlO_{10})(OH)_2 + 10H^+ \rightarrow K^+ + 3Al^{3+} + 3Si(OH)_4 \quad (10)$$

$$(Ca_{0.22}Mg_{2.18})(Mg_{0.7}Fe_{2.3}Al)(Al_{1.8}Si_{6.2})O_{20}(OH)_4 + 19.2H^+ + 0.8H_2O \rightarrow 22Ca^{2+} + 2.88Mg^{2+} + 2.3Fe^{2+} + 2.8Al^{3+} + 6.2H_4SiO_4 \quad (11)$$

$$K_{1.26}(Mg_{0.02}Fe_{0.19}Al_{3.80})(Al_{1.26}Si_{6.75})O_{20}(OH)_4 + 16.86H^+ + 3.07H_2O \rightarrow 26K^+ + 0.02Mg^{2+} + 0.19Fe^{2+} + 5.06Al^{3+} + 6.75H_4SiO_4 \quad (12)$$

$$Na_{0.93}Ca_{0.07}Al_{1.07}Si_{2.93}O_8 + 4.28H^+ + 3.72H_2O \rightarrow 0.93Na^+ + 0.07Ca^{2+} + 1.07Al^{3+} + 2.93H_4SiO_4 \quad (13)$$

$$KAlSi_3O_8 + 4H^+ + 4H_2O \rightarrow K^+ + Al^{3+} + 3H_4SiO_4 \quad (14)$$

$$SiO_2 + H_2O \rightarrow H_4SiO_4 \quad (15)$$

Eqs. (7)–(15) represent the simplest case in which complete dissolution occurs. However, as a result of incongruent dissolution, different elements can be released at different rates from the same mineral, resulting in significantly more complicated dissolution reactions. No attempt was made to correct the phyllosilicates for incongruent dissolution. In case of these minerals, the rate was either calculated from an element with an intermediate release rate, or congruent dissolution was reached fairly early in the leach.

It was not possible to treat the tectosilicates with this simple approach. Feldspar release rates were determined using the relative release ratios of Stillings and Brantley (1995). There was no quantitative data published for laumontite and it was therefore

Table 3
Estimated mean surface areas (A) calculated from stereologically corrected gangue mineral grain sizes and roughness data (R_s).

Sample	MKB1-212 (m^2/g)		MKB1-75 (m^2/g)		RAO (m^2/g)		OAO (m^2/g)		MSO (m^2/g)	
Determination	A	R_s	A	R_s	A	R_s	A	R_s	A	R_s
Quartz	–	–	–	–	–	–	–	–	–	–
Plagioclase[a]	0.67	11.14	1.18	11.32	1.02	11.06	0.65	10.38	0.39	11.89
K-feldspar[a]	0.63	11.32	1.04	11.37	0.99	11.72	0.67	11.56	2.48	11.97
Laumontit	0.11	1.00	0.17	1.00	–	–	–	–	–	–
Muscovite[b]	1.96	13.77	3.43	13.78	1.04	13.87	2.91	13.89	–	–
Chlorite[c]	2.18	6.17	2.89	6.15	1.61	6.15	–	–	–	–
Smectite	–	–	–	–	–	–	–	–	–	–
Illite	–	–	–	–	–	–	–	–	–	–
Calcite[d]	0.22	2.48	0.33	2.48	–	–	–	–	–	–

[a] Feldspar roughness calculated using data from Knauss and Wolery (1986), Casey et al. (1991), Stillings and Brantley (1995) and Chen and Brantley (1997).
[b] Muscovite roughness calculated using data from Nickel (1973), Knauss and Wolery (1989) and Kalendova et al. (2010).
[c] Chlorite roughness calculated using data from Brandt et al. (2003), Lowson et al. (2005) and Hen et al. (2007).
[d] Calcite roughness calculated using data from Anderson (1968), Oleg et al. (2005) and Oelkers et al. (2011).

Table 4
Uranium deportment, determined by QEMScan TMS, detailing the proportion of the total contained uranium hosted by each uranium mineral.

Sample	MKB1-212 (%)	MKB1-75	MKB1 (Ave) (%)	RAO (%)	OAO (%)	MSO (%)
Uraninite	23.92	19.30	21.61	4.87	24.79	–
Coffinite	74.60	77.95	76.28	65.18	74.03	–
Uraniferous leucoxene	0.44	1.16	0.80	29.95	1.17	–
Thorite	1.04	1.59	1.31	–	–	–
Meta-uranocircite	–	–	–	–	–	54.65
Meta-autunite	–	–	–	–	–	45.35
Total	100.00	100.00	100.00	100.00	100.00	100.00

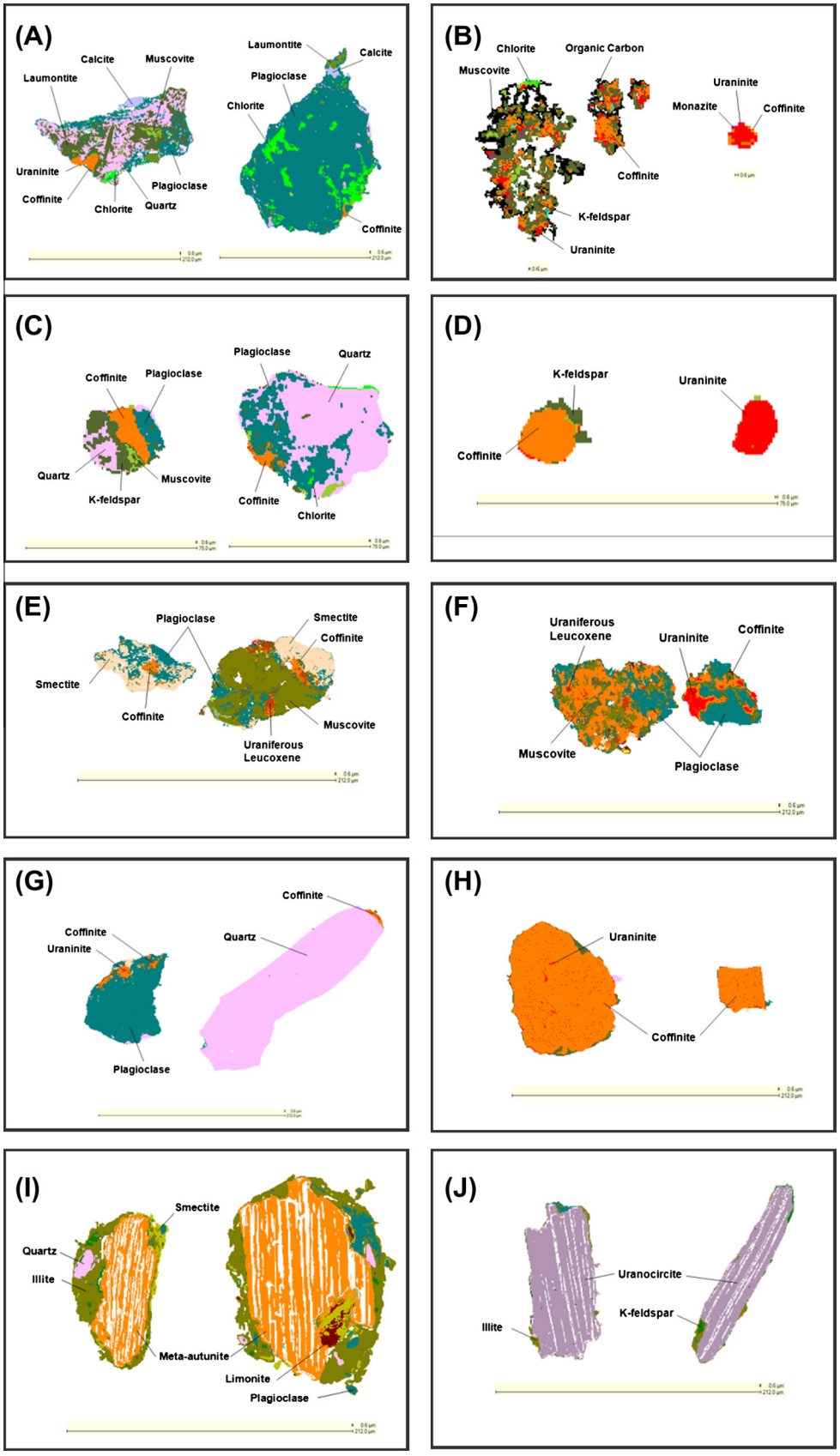

Fig. 1. QEMScan TMS particle maps showing U minerals from MKB1-212 (A and B), MKB1-75 (C and D), RAO (E and F), OAO (G and H) and MSO (I and J). The large scale bars in all except B, C and D are 212 μm. Those in B are 0.6 μm, while those in C and D are 75 μm.

Table 5
Uranium mineral exposure and association characteristics as determined by QEMScan TMS.

Sample exposure and association categories	MKB1-212 (Mass%)	MKB1-75 (Mass%)	RAO (Mass%)	OAO (Mass%)	MSO (Mass%)
Exposed	69.71	90.86	64.38	91.79	93.63
Locked in reactive minerals	5.94	2.02	20.90	3.11	6.33
Locked in low reactivity minerals	24.34	7.12	14.71	5.10	0.04
Total	100.00	100.00	100.00	100.00	100.00

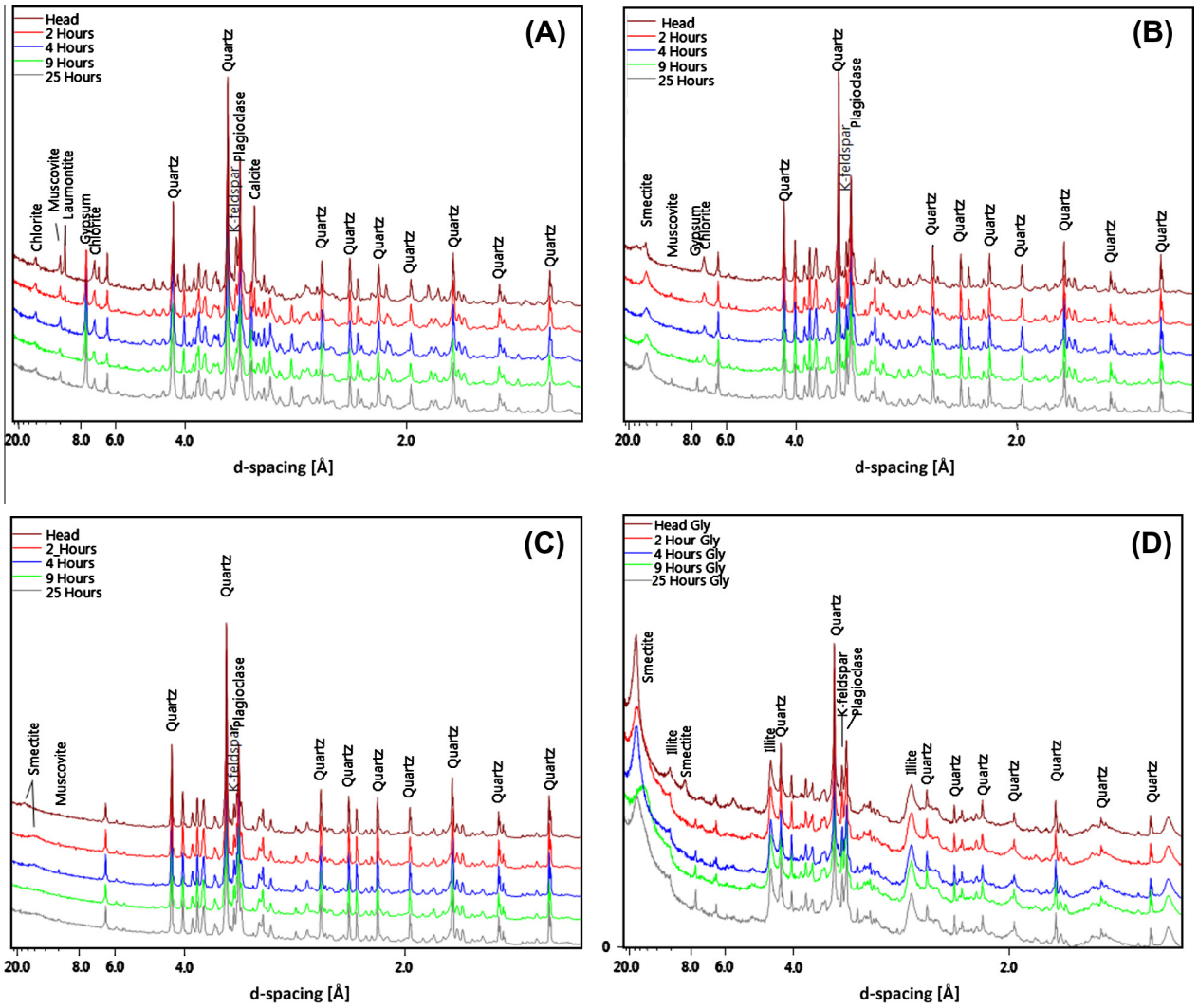

Fig. 2. X-ray diffractograms showing the change in gangue mineralogy as the leaches progress. In each case diffractograms are in sequential order, with the head sample as the upper diffractogram and the 25 h residue is the lowest. (A–D) represent the diffractograms collected from MKB1, RAO, OAO and MSO respectively.

necessary to determine these as part of the present study. Using these results the acid consumption characteristics of the tectosilicates were determined. The ideal acid consumption characteristics of selected minerals are given in Table 1. Where necessary, the acid consumption corrected for incongruent dissolution has also been given. These values, when multiplied by the mass percent of the mineral that dissolved during the leach (calculated as the mass of dissolved mineral relative to the mass of ore treated), can be used to calculate the amount of acid consumed in the dissolution of that phase.

Manganese dioxide is the second reagent used in the U leaches. The dissolution of this reagent also consumes acid according to Eq. (2). It is therefore necessary to be able to accurately predict the MnO_2 demand of an ore. There was insufficient literature on MnO_2 in U leaching to predict the MnO_2 consumption. It was therefore necessary to produce an equation for this purpose from the results of this study.

3.4. Free acid

In this case free acid concentration refers to the acid that remains in solution to maintain the low pH needed for U dissolution. Eq. (16) gives the relationship between H^+ activity and pH, and Eq. (17) gives the relationship between activity and concentration (Harris, 1999).

$$pH = -\log a_{H+} \tag{16}$$

$$A_c = [C]\gamma_c \tag{17}$$

Table 6
Leach conditions and uranium dissolution.

Test	Sample	P_{80}	pH	Eh	U dissolution (%)*
A	MKB1	212	0.97	499	89.47
B	MKB1	212	1.52	449	70.36
C	MKB1	75	1.51	457	86.80
D	MKB1	212	2.02	413	67.71
E	RAO	212	1.56	428	85.13
F	OAO	212	1.47	485	83.06
G	MSO	212	1.33	471	88.44

* Duplicate leach tests suggest that the error in the U dissolution is 3.89%.

where A_c is the activity of ion C, $[C]$ is the concentration (in mol/L) of C and γ_c is the activity coefficient. There are a number of methods of determining the activity coefficient. These include the Debye–Hückel method, which can be used to determine the activity coefficient for solutions with an ionic strength less than 0.1 mol/L (Harris, 1999). Due to the high ionic strengths that can be reached in U PLS, it was decided to use the Davies method (as recommended by Samson et al., 1999).

Both the Debye–Hückel and the Davies method are based on the ionic strength of the solution, which is a function of solution composition. The dissolution data obtained using Eq. (4) and Eqs. (7)–(15) were used to determine the ion input into solution. However, the composition of the solution (and therefore the ionic strength) differs from this input composition for two reasons. The first involves the formation of gypsum (Danielle et al., 2008) which removes both Ca^{2+} and SO_4^{2-} from solution in equal molar quantities. The second involves the formation of ion pairs in solution (Reardon and Langmuir, 1976). The solubility of gypsum and concentrations of the ion pairs are determined according to Eqs. (18) and (19) respectively.

$$Ksp_{gypsum} = A_{Ca^{2+}} \times A_{SO_4^{2-}} \tag{18}$$

$$K_{CaSO_4} = \frac{A_{Ca^{2+}} \times A_{SO_4^{2-}}}{A_{CaSO_4}} \tag{19}$$

where Ksp_{gypsum} is the solubility product constant of gypsum, A_i is the activity of the respective species (equal to the product of the activity constant and the concentration), and K_{CaSO4} is the equilibrium constant for the formation of calcium sulphate ion pairs. Typical values for Ksp_{gypsum} range from $10^{-4.59}$ to $10^{-4.35}$ while K_{CaSO4} has a value of $10^{-2.31}$ (Reardon and Langmuir, 1976 and Messnaoui and Bounahmidi, 2006).

In addition to the activity coefficient, it is also necessary to consider the second acid dissociation of sulphuric acid. The higher the acid consumption of the ore, the more SO_4^{2-} accumulates in solution (except where precipitates such as gypsum form). The increased levels of SO_4^{2-} forces the dissociation reaction to the left, forming HSO_4^- at the expense of H^+. For ores with high acid consumptions, the second dissociation of sulphuric acid is even more significant than the hydrogen ion activity coefficient.

An Excel-based model was developed that considers the dissolution of each major mineral phase, the MnO_2 addition, the solution composition, gypsum and ion pair formation, ionic strength and activity coefficients, the free acid demand and the concentrations of the HSO_4^- ion in solution. Due to the interdependence of the variables in the model, an iterative approach was used. The first iteration assumed that the activities of the various species equalled their concentration. Later iterations considered the activity coefficients. The model typically required four iterations to stabilise.

4. Results

4.1. Head sample gangue mineral characterisation

The XRD and BMA analyses produced very comparable gangue mineral abundances and the composition of each sample is given in Table 2. The arkose from the main Karoo basin (MKB1), the Kayelekera reduced arkose ore (RAO) and oxidised arkose ore (OAO) consist of subequal amounts of quartz and plagioclase with lesser K-feldspar. MKB1 also contains calcite, laumontite, chlorite and muscovite. The RAO also contains chlorite and pyrite. RAO and OAO contain smectite, but the highest smectite concentrations oc-

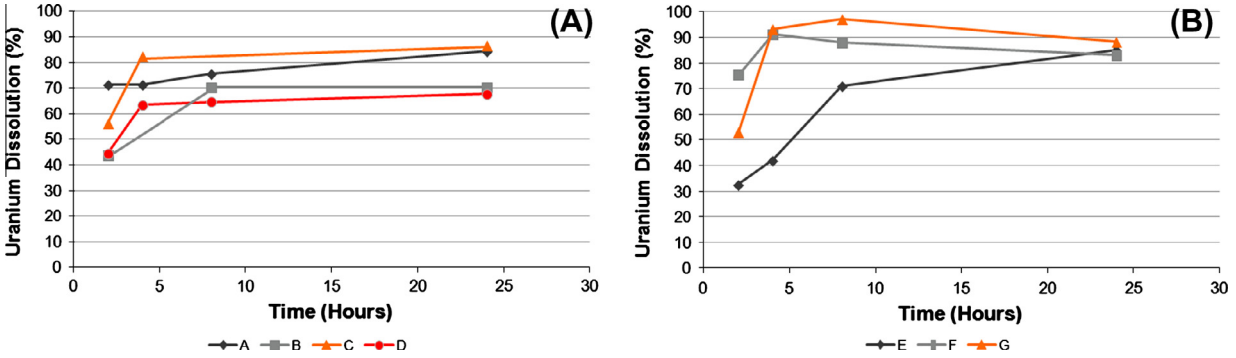

Fig. 3. Uranium dissolution as a function of time. The MKB leaches (tests A–D) are shown to the left in (A) and tests E to G (the Kayelekera leaches) are shown to the right in (B). Based on the results of duplicate leach tests, the error in dissolution is estimated to be 3.89%.

Table 7
Ore ferrous iron concentrations, leach conditions, measured and calculated manganese dioxide consumptions.

Test	Sample	Fe^{2+}	pH	Eh	MnO_2 Meas (kg/ton)	MnO_2 Calc. (kg/ton)
A	MKB1	0.83	0.97	499	17.88	12.1
B	MKB1	0.83	1.52	449	6.94	6.8
C	MKB1	0.83	1.51	457	11.69	7.6
D	MKB1	0.83	2.02	413	2.93	2.9
E	RAO	4.52	1.56	428	32.93	32.9
F	OAO	0.48	1.47	485	1.45	1.5
G	MSO	0.48	1.33	471	0.00	0.0

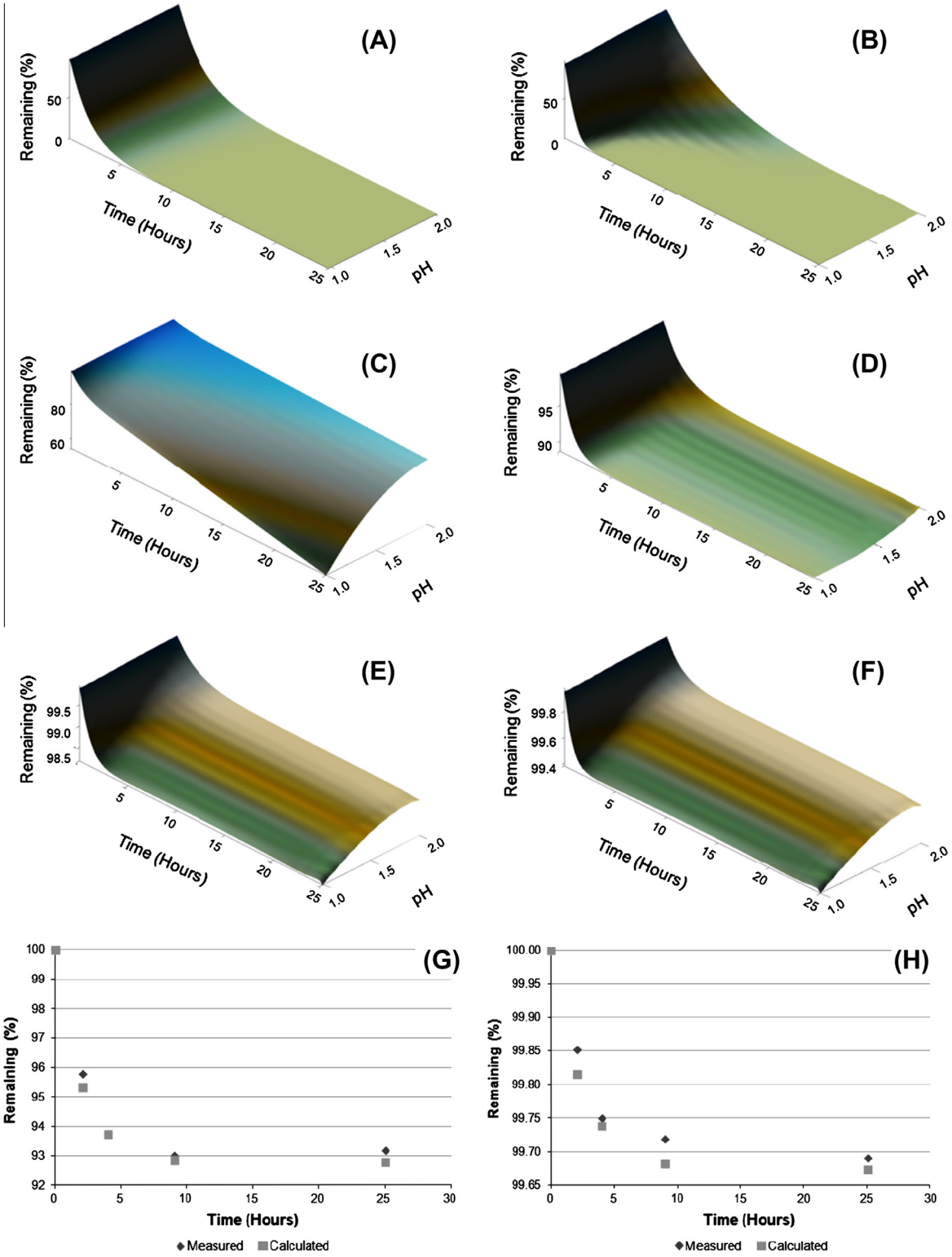

Fig. 4. Modelled acid dissolution of calcite (A), laumontite (B), chlorite (C), muscovite (D), plagioclase (E) and K-feldspar (F) expressed as a function of pH and time. Measured and calculated smectite (G) and illite (H) dissolution are also shown; however these are only expressed as a function of time. It was not possible to determine the dissolution characteristics of smectite and illite as a function of pH because the samples that contain these minerals were only leached at ~pH 1.5.

cur in MSO. The dominant phase in MSO is illite, with lesser plagioclase and minor K-feldspar and quartz.

Stereologically corrected grain sizes indicate that in each sample, quartz is the coarsest phase, followed by plagioclase and then K-feldspar in the Kayelekera samples. In the MKB1 sample calcite is the second coarsest phase (at both grinds). Estimated specific surface areas were needed for the surface area normalisation of the rates. These values (calculated from the grain size data) are presented in Table 3. For reference the surface roughness values used in the calculations are also shown.

4.2. Uranium mineral characterisation

The MKB1 sample had a head grade of 208 ppm U_3O_8. Both RAO and MSO have significantly higher U grades (2369 ppm and 1635 ppm U_3O_8 respectively), while OAO only has a grade of 387 ppm U_3O_8.

The U deportments of MKB1 and OAO are similar (Table 4 and Fig. 1). In these samples the majority of the U is present in coffinite ($U(SiO_4)_{1-x}(OH)_{4x}$) with lesser amounts occurring in uraninite (UO_2). RAO differs from these samples in that uraniferous leucoxene, rather than uraninite, is the second most important U mineral. The U deportment of MSO is completely different from any of the arkose samples, with subequal amounts of U occurring in meta-uranocircite ($Ba(UO_2)_2(PO_4)_2{\cdot}6H_2O$) and meta-autunite ($Ca(UO_2)_2(PO_4)_2{\cdot}6H_2O$).

The exposure and association characteristics of each sample are summarised in Table 5. Exposed grains are those that have a proportion of their surface that is exposed at the edge of a particle. These are grains that would be available for dissolution. MKB1 exposure was not particularly high at 80% passing 212 μm and ~24% of U mineral grains are locked in low reactivity gangue. However, there was a significant improvement in exposure at 80% passing 75 μm, where only ~7% of U mineral grains occur in low reactivity gangue. The proposition of exposed grains in RAO was also low (~64%), however a significant amount of the locked grains occur within reactive gangue.

The exposures of OAO and MSO were both high, with ~92% of grains in OAO and ~94% in MSO showing some degree of exposure.

4.3. Analysis of leach products

X-ray diffractograms showing changes in the gangue mineralogy, in response to acid leaching, are given in Fig. 2. Only one of the MKB1 leaches has been shown. This leach was at a P_{80} of 212 and a pH of 1.52. The other leaches show similar trends, except that the leaches at lower pH or finer grind show more rapid gangue dissolution, while the leach at higher pH showed slower dissolution.

The most noticeable changes in the mineralogy of the MKB1 sample (Fig. 2A) is the disappearance of calcite and laumontite, the depletion of chlorite and the formation of gypsum. Trace amounts of gypsum also formed in the residues of RAO (Fig. 2B). RAO also showed depletion of chlorite and changes in the shape and position of the smectite peak.

Variation in the smectite peak shape and position were the only changes seen in the residues of OAO (Fig. 2C). However, these changes are more clearly seen in MSO (Fig. 2D) where the higher smectite concentration made the changes more obvious. It can be seen that the interlayer spacing of the smectite progressively collapses from 17.1 Å in the head sample to 14.4 Å in the 9 h residue. This is accompanied by a marked broadening of the peak. However, in the 25 h residue, the interlayer spacing increases to 16.7 Å, with a significantly narrower peak than in the 9 h residue.

The U dissolutions at the end of the 24 h leach period are given in Table 6; the leach conditions are also shown. Fig. 3A shows the U dissolution curves for the four MKB1 leaches and Fig. 3B shows the Kayelekera leaches. Two data points are missing from Fig. 3A. These are Test B, 4 h and Test C, 9 h. Due to the high concentrations of silica (resulting from zeolite dissolution), the MKB1 samples gelled after a few days. This gelling occurred before it was possible to complete the analyses of the PLS for these two points.

In the MKB1 leaches, Tests A and C showed very similar dissolutions, with progressively lower dissolution in B and D. The Kayelekera dissolutions were all above 80%, with dissolutions increasing from OAO through RAO to MSO. However, examination of the dissolution curves (Fig. 3B) show that OAO reached maximum dissolution (of 91.21%) at 4 h and MSO reached maximum dissolution (of 97.31%) at 9 h. Thereafter, both samples show a decrease in the percentage U dissolution.

5. Modelling of gangue dissolution

Using the results of the Fe^{2+} titrations on the head samples, the MnO_2 consumptions and the redox potential of the leach tests, Eq. (20) was found to predict the MnO_2 consumption with reasonable accuracy (Table 7). However, as shown in Eq. (2) the consumption of MnO_2 involves Fe^{2+} in the PLS and therefore Eq. (20) relies on the assumption that the Fe^{2+} dissolution characteristics, of an ore, are the same as those in this study. Since Fe dissolution is a function of pH, Eq. (20) also assumes a relationship between the pH and

Table 8
Variables used in modelling gangue dissolution in Eqs. (21)–(23) as well as their measures of fit.

Mineral	Variable[a]	*a*	*b*	*c*	Measure of fit[b]
Calcite	R_0	30.48	−155.89	396.53	0.947
	$-\lambda$	−0.08	0.38	−0.89	
	z	0.00	0.00	0.00	
Laumontite	R_0	878.27	−3605.07	3870.56	0.981
	$-\lambda$	−0.79	3.25	−3.50	
	z	0.00	0.00	0.00	
Chlorite	R_0	6.35	−23.10	21.92	0.991
	$-\lambda$	0.00	0.00	−0.95	
	z	0.42	−1.83	2.04	
Muscovite	R_0	−2.93	4.56	4.83	0.923
	$-\lambda$	0.54	−1.07	−0.57	
	z	0.00	0.00	0.00	
Plagioclase	R_0	1.75	−7.99	9.61	0.854
	$-\lambda$	0.43	−0.53	−1.09	
	z	0.00	0.00	0.00	
K-feldspar	R_0	1.21	−5.08	5.67	0.994
	$-\lambda$	0.46	−0.17	−2.13	
	z	0.00	0.00	0.00	

[a] Both R_0 and *z* are given in terms of the proportion of the mineral of interest (expressed as a percentage) dissolved per hour normalised to the specific surface area or percent/(m^2/g h).
[b] The measure of fit was obtained by comparing the measured mineral dissolution data with calculated dissolution data. The parameter used above is the square of the correlation coefficient.

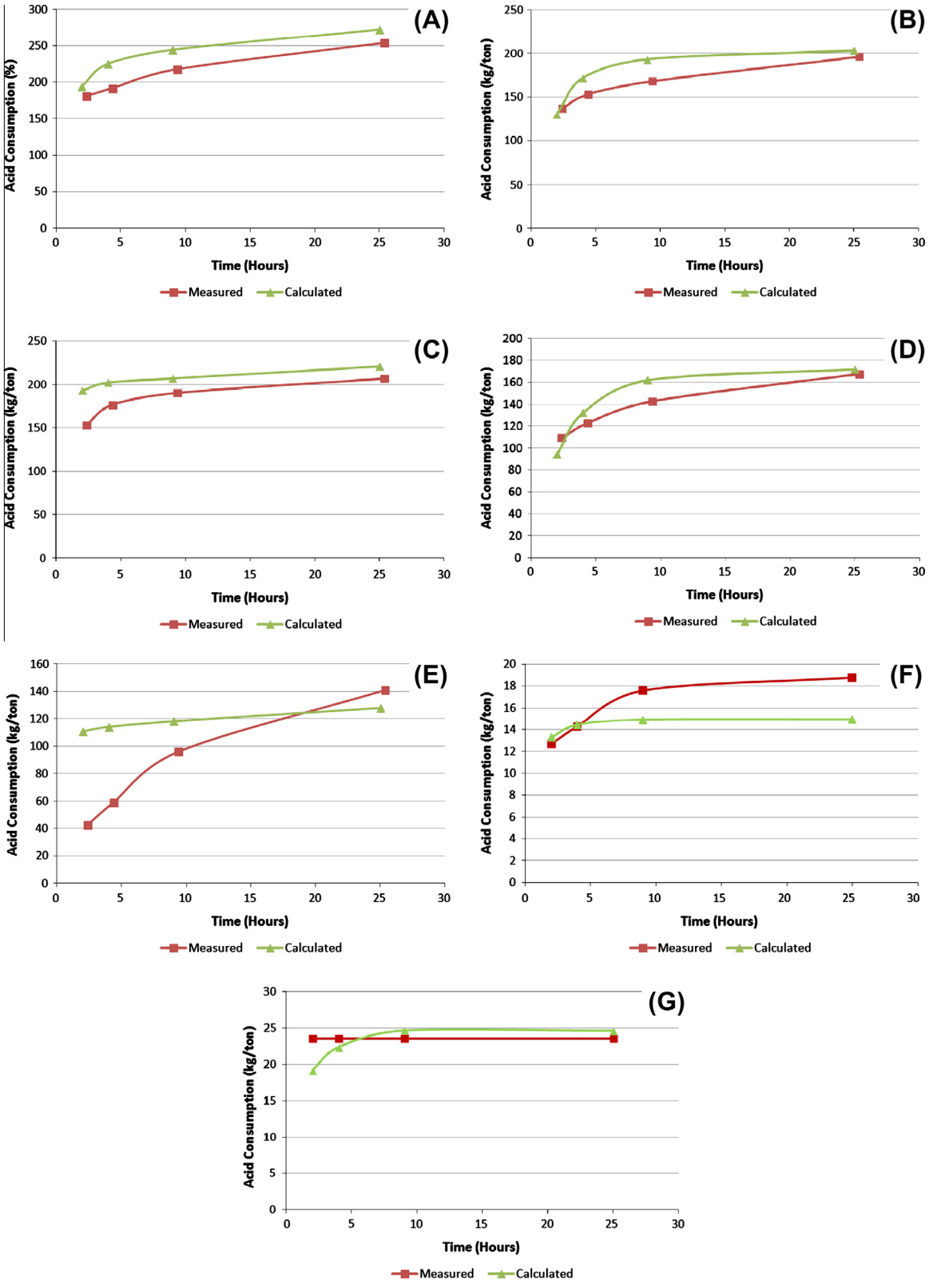

Fig. 5. A comparison of the acid consumed in each of the leaches with the amount predicted by the model. Plots (A–G) represent leaches A–G respectively (see Table 7 for the conditions of each leach). In several of the plots, especially (E), there is a large discrepancy between the measured and calculated data in the early hours of the leach. This is because the model assumed all the MnO_2 was added at the first hour, while in the leach tests the MnO_2 was added progressively throughout the leach. Duplicate leach tests suggest that the error in the measured acid consumption is 4.91%, while the average error in the calculated acid consumption (determined by comparing the measured and calculated acid consumptions) is ~8%.

Eh conditions used in the leach. The assumption being that when more oxidising conditions are used, then the leaches would also be performed at lower pH.

$$MnO_2 = 38.58 \log[Fe^{2+}] + 0.1069\ Eh - 38.09 \quad (20)$$

The modelled dissolutions of the various gangue phases are shown in Fig. 4. For most minerals the dissolutions are shown as a function of both time and pH. However, because the samples that contained smectite and illite were all leached at approximately pH 1.5, it was not possible to plot the dissolution of these minerals in pH-time space. These were plotted as a function of time at pH 1.5.

The variables and a measure of fit, comparing the modelled and measured dissolution data for each mineral (except smectite and illite), are given in Table 8. The variables used for smectite were 3.60 for R_0, −0.50 for $-\lambda$ and 0 for z. Those used for illite were 0.0031 for R_0, −0.40 for $-\lambda$ and 0 for z.

$$R_0 = a_1\ pH^2 + b_1\ pH + c_1 \quad (21)$$

$$-\lambda = a_2\ pH^2 + b_2\ pH + c_2 \quad (22)$$

$$z = a_3\ pH^2 + b_3\ pH + c_3 \quad (23)$$

The results of the measured acid consumptions, compared with those predicted by the model are shown in Fig. 5. The Eh control was maintained by addition of MnO_2, which is an important acid consumer. However, due to the slow dissolution of MnO_2, it was necessary to add small amounts and then monitor the changes in Eh over time. It was, therefore, not possible to add all of the necessary MnO_2 at the start of the leach. The model assumes that all MnO_2 was added after the hour of preconditioning and for this reason there is a discrepancy between the measured and calculated acid consumptions in the early stages of the leach (especially for Test E). Besides the MnO_2 discrepancy, the calculated acid consumptions closely approximate the measured consumptions.

6. Discussion

6.1. Uranium dissolution

A comparison of the MKB1 exposure data (Table 5) obtained by QEMScan TMS, with U dissolution in the leach tests (Table 6) found that, in tests B and D, the amount of exposed U agreed well with the percentage U dissolution. The finer grind used in test C allowed for significantly higher U dissolution and again there was agreement between the exposure and dissolution data. However, the dissolution seen in Test A far exceeds the predicted value based on the U mineral exposure. In order to achieve such high dissolutions, significant amounts of locked U must have been exposed by the aggressive conditions of the leach.

The U minerals in OAO and MSO both had very high degrees of exposure (>91%), but the final U dissolution in these samples was less than 89%. The maximum dissolution in both of these samples was not achieved at 24 h, with OAO reaching a maximum dissolution of ~91% at 4 h and MSO reaching maximum dissolution (~97%) at 9 h. After these maxima, both leaches showed progressive decreases in U dissolution. This could either be the result of U precipitation from solution, or may be due to the smectite.

Both of these samples contain smectite. XRD analysis of the leach residues show a progressive collapse in the interlayer spacing of the smectite from the head sample (at ~17 Å) to the 9 h residue where it reached ~14 Å). Thereafter the interlayer spacing increased, reaching ~17 Å in the 25 h residue. It is possible that the interlayer collapse is the result of H^+ replacement of the interlayer cations. Then as the ionic strength of the solutions increased, other larger cations (including U) became available for substitution. The substitution of these cations could have resulted in the increase in the interlayer spacing. This substitution may also be the reason for the decrease in U dissolution in the later stages of the leach.

OAO and MSO were not the only samples to contain smectite. RAO contained more smectite than OAO, but this sample did not show the same decrease in dissolution in the later stages of the leach. There are two likely reasons. The first is that in RAO ~20% of the U occurred in grains locked in reactive gangue. This U was released more slowly as time was required to dissolve the gangue. This prevented this leach from developing an early maximum. The second is that the RAO solution contained very high concentrations of other elements, especially Mn from the oxidiser. These elements may have preferentially substituted into the smectite.

6.2. Gangue dissolution

The dissolution characteristics of several common gangue minerals were determined. These results show that gangue dissolution increases with decreasing pH and grain size. The rate of dissolution of most minerals follows an exponential decay function, from an initially rapid rate to a much slower one as the leach progresses.

The dissolution rates of calcite and laumontite are rapid and both phases were completely dissolved, (although laumontite is subject to incongruent dissolution and it is likely that an amorphous Si–Al solid phase is still present in the residues at the end of the leach).

Chlorite dissolution was also rapid, but not as rapid as that of calcite or laumontite. Depending on the pH and specific surface area, between about 7% and 47% of the contained chlorite can dissolve within the duration of an acid leach. Muscovite dissolution was much slower and only about 12% dissolved at pH 0.97. While the feldspars do dissolve, the rate of this dissolution was very slow. Neither plagioclase nor K-feldspar showed more than 2% dissolution.

Considering both the rate at which gangue phases dissolve, and the amount of acid they consume during dissolution, carbonates are the most aggressive gangue acid consumers, followed by laumontite (although this phase does not occur in many U deposits) and chlorite. Muscovite, smectite and illite were moderate acid consumers, while only minor dissolution of plagioclase and K-feldspar dissolved. The dissolution characteristics of these minerals can be used both in assessing the reagent consumption of an ore and the effect of U mineral texture (particularly exposure and association) on U dissolution.

7. Conclusions

The following conclusions can be drawn from the results of this study:

(1) The dissolution of gangue minerals can result in substantial increases in U mineral dissolution.
(2) The presence of smectite can result in the loss of U from solution as the leach progresses. High concentrations of zeolite in the ore can also be deleterious both increasing acid consumption and causing gelling of the PLS.
(3) It is possible to estimate the percentage U dissolution, during acid leaching, from QEMScan TMS data. For a non-refractory ore, at moderate conditions (pH ~1.5, 35–40° C, 24 h duration) the percentage U dissolution approximately equals the proportion of the U mineral grains that show some degree of exposure. At lower pH conditions (~1.0) the U dissolution may exceed the sum of exposed U grains

and those associated with reactive gangue. At higher pH (~2.0) the U dissolution is lower than the proportion of exposed grains (presumably due to slow leach kinetics).

(4) Provided detailed data are available, it is possible to use mineralogical data to predict the acid dissolution characteristics of gangue minerals with reasonable accuracy. These predictions can be used in conjunction with free acid calculations to predict the acid consumption characteristics of the ore. To estimate the gangue acid consumption of a particular ore, the values in Table 8 can be used. For more accurate data, these values should be calibrated for a particular U deposit by comparison of mineralogical and leach test data. Similarly Eq. (20) may need to be calibrated for a particular deposit.

Acknowledgements

The authors would like to thank Paladin Energy for contributing most of the U ore used in this study and SGS South Africa for sponsoring instrument and batch reactor time. The advice of Johan O' Connell, Louis Coetzee, Maria Klaas and Annegret Lombard is also greatly appreciated.

References

Abhilash, S., Singh, K.D., Mehta, V., Kumar, B.D., Pandey, V.M., 2009. Dissolution of uranium from silicate-apatite ore by *Acidithiobacillus ferrooxidans*. Hydrometallurgy 95, 70–75.

Amram, K., Ganor, J., 2005. The combined effect of pH and temperature on smectite dissolution rate under acidic conditions. Geochimica et Cosmochimica Acta 69, 2535–2546.

Anderson, T.F., 1968. Surface area measurement in calcite grains by isotopic exchange with C^{14} labelled carbon dioxide. Geochimica et Cosmochimica Acta 32, 1177–1186.

Bibi, I., Singh, B., Silvester, E., 2011. Dissolution of illite in saline–acidic solutions at 25°C. Geochimica et Cosmochimica Acta 75, 3237–3249.

Blum, A.E., Yund, R.A., Lasaga, A.C., 1990. The effect of dislocation density on the dissolution rate of quartz. Geochimica et Cosmochimica Acta 54, 283–297.

Brandt, F., Bosbach, D., Krawczyk-Bärch, E., Arnold, T., Bernhard, G., 2003. Chlorite dissolution in the acid pH-range: a combined microscopic and macroscopic approach. Geochimica et Cosmochimica Act 67, 1451–1461.

Brantley, S.L., 2008. Kinetics of mineral dissolution. In: Brantley, S.L., Kubicki, J.D., White, A.F. (Eds.), Kinetics of Water–Rock Interactions. Springer Science, pp. 151–210.

Brantley, S.L., Conrad, C.F., 2008. Analysis of rates of geochemical reactions. In: Brantley, S.L., Kubicki, J.D., White, A.F. (Eds.), Kinetics of Water–Rock Interactions. Springer Science, pp. 1–37.

Brown, T.L., LeMay, H.E., Bursten, B.E., 2003. Chemistry the Central Science, nineth ed. Prentice Hall, New Jersey, p. 635.

Brunauer, S., Emmett, P.H., Teller, E., 1938. Adsorption of gases in multimolecular layers. Journal of the American Chemical Society 60, 309–319.

Casey, W.H., Westrich, H.R., Holdren, G.R., 1991. Dissolution rates of plagioclase at pH = 2 and 3. American Mineralogist 76, 211–217.

Chen, Y., Brantley, S.L., 1997. Temperature – and pH dependence of albite dissolution rate at acid pH. Chemical Geology 135, 275–290.

Coetzee, L., Theron, S.J., Martin, G.J., van der Merwe, J., Stanek, T., 2011. Modern gold deportments and its application to industry. Minerals Engineering 24, 565–575.

Danielle, M.C., Huminicki, J., Rimstidt, D., 2008. Neutralization of sulphuric acid solutions by calcite dissolution and the application to anoxic limestone drain design. Applied Geochemistry 23, 148–165.

Gottlieb, P., Wilkie, G., Sutherland, D., Ho-Tun, E., Suthers, S., Perera, K., Jenkins, B., Spencer, S., Butcher, A., Rayner, J., 2000. Using quantitative electron microscopy for process mineralogy applications. Journal of the Minerals, Metals and Materials Society 52, 24–25.

Harris, D.C., 1999. Quantitative Chemical Analysis, 5th Ed. W.H. Freeman and Co., New York, pp 129–212.

Helgeson, H.C., Murphy, W.M., Aaraard, P., 1984. Thermodynamic and kinetic constraints on reaction rates among minerals and aqueous solutions. II. Rate constants, effective surface area, and hydrolysis of feldspar. Geochimica et Cosmochimica Acta 48, 2405–2432.

Hen, F., Durand, C., Cerepi, A., Brosse, E., Giuntini, J.C., 2007. DC conductivity, cation exchange capacity, and specific surface area related to chemical composition of pore lining chlorites. Journal of Colloid and Interface Science 311, 571–578.

HO, E.M., Quan, H., 2007. Iron (II) oxidation by SO2/O2 for use in uranium leaching. Hydrometallurgy 85, 183–192.

Hodson, M.E., 2006. Searching for the perfect surface area normalizing term – a comparison of BET surface area-, geometric surface area- and mass normalized dissolution rates of anorthite and biotite. Journal of Geochemical Exploration 88, 288–291.

IAEA, 1980. Significance of Mineralogy in the Development of Flowsheets for Processing of Uranium Ores. International Atomic Energy Agency, Vienna, pp. 1–161.

IAEA, 1990. Manual on Laboratory Testing for Uranium Ore Processing. International Atomic Energy Agency, Vienna, pp. 1–127.

Kalendova, A., Vesely, D., Kalenda, P., 2010. Properties of paints with hematite coated muscovite and talc particles. Applied Clay Science 48, 581–588.

Knauss, K.G., Wolery, T.J., 1986. Dependance of albite dissolution kinetics on pH and time at 25 °C and 75 °C. Geochimica et Cosmochimica Acta 50, 2481–2497.

Knauss, K.G., Wolery, T.J., 1989. Muscovite dissolution kinetics as a function of pH and time at 70 °C. Geochimica et Cosmochimica Acta 53, 1493–1501.

Kohler, S., Dufaud, F., Oelkers, E.H., 2003. An experimental study of illite dissolution kinetics as a function of pH from 1.4 to 12.4 and temperature from 5 to 50 °C. Geochimica et Cosmochimica Acta 67, 3583–3594.

Lottering, M.J., Lorenzen, L., Phala, N.S., Smit, J.T., Schalkwyk, G.A.C., 2008. Mineralogy and uranium leaching response of low grade South African ores. Minerals Engineering 21, 16–22.

Lowson, R.T., Comarmond, J.M.C., Rajaratnam, G., Brown, P.L., 2005. The kinetics of the dissolution of chlorite as a function of pH and at 25 °C. Geochimica et Cosmochimica Acta 69, 1687–1699.

Lunt, D., Boshoff, P., Boylett, M., El-Ansary, Z., 2007. Uranium extraction: the key process drivers. The Journal of the South African Institute of Mining and Metallugy 107, 419–426.

Lüttge, A., Arvidson, R.S., 2008. The Mineral-Water Interface. In: Brantley, S.L., Kubicki, J.D., White, A.F. (Eds.), Kinetics of Water–Rock Interactions. Springer Science, pp. 82–83.

McCusker, L.B., Von Dreele, R.B., Cox, D.E., Louër, D., Scardi, P., 1999. Rietveld refinement guidelines. Journal of Applied Crystallography 32, 36–50.

Merritt, R.C., 1971. The Extractive Metallurgy of Uranium. Colorado School of Mines. Under Contract with the United States Atomic Energy Commission, 60–86.

Messnaoui, B., Bounahmidi, T., 2006. On the modelling of calcium sulphate solubility in aqueous solutions. Fluid Phase Equilibria 244, 117–127.

Metz, V., Amram, K., Ganor, J., 2005. Stoichiometry of smectite dissolution. Geochimica et Cosmochimica Acta 69, 1755–1772.

Miki, H., Nicol, M., 2009. The kinetics of the oxidation of iron (II) by chlorate in the leaching of uranium ores. Hydrometallurgy 100, 47–49.

Nickel, E., 1973. Experimental dissolution of light and heavy minerals in comparison with weathering and intrastratal solution. Contributions to Sedimentology 1, 1–68.

Oelkers, E.H., Schott, J., Gauthier, J., Herrero-Roncal, T., 2008. An experimental study of the dissolution mechanism and rates of muscovite. Geochimica et Cosmochimica Acta 72, 4948–4961.

Oelkers, E.H., Golubev, S.V., Pokrovsky, O.S., Benezeth, P., 2011. Do organic ligands affect calcite dissolution rates? Geochimica et Cosmochimica Acta 75, 1799–1813.

Oleg, S.P., Sergey, V.G., Schott, J., 2005. Dissolution kinetics of calcite, dolomite and magnesite at 25°°C and 0 to 50 atm pCO_2. Chemical Geology 217, 239–255.

Reardon, E.J., Langmuir, D., 1976. Activity coefficients of $MgCO_3$ can $CaSO_4$ ion pairs as a function of ionic strength. Geochimica et Cosmoshimica Acta 40, 549–554.

Ross, G.J., 1969. Acid dissolution of chlorites: release of magnesim, iron and aluminium and mode of acid attach. Clays and Clay Minerals 17, 347–354.

Samson, E., Lemaire, G., Marchand, J., Beaudoin, J.J., 1999. Modeling chemical activity effects in strong ionic solutions. Computational Materials Science 15, 285–294.

Serway, R.A., Faughn, J.S., 2003. College Physics, Sixth ed. Thomson, 906.

Stillings, L.S., Brantley, S.L., 1995. Feldspar dissolution at 25 °C and pH 3: reaction stoichiometry and the effect of cations. Geochimica et Cosmochimica Acta 59, 1483–1496.

Sutherland, D., Gottlieb, P., Jackson, R., Wilkie, G., Stewart, P., 1988. Measurement in section of particles of known composition. Minerals Engineering 1, 317–326.

Tester, J.W., Worley, W.G., Robinson, B.A., Grigsby, C.O., Feerer, J.L., 1994. Correlating quartz dissolution kinetics in pure water from 25 to 625 °C. Geochimica et Cosmochimica Acta 58, 2407–2420.

Venter, R., Boylett, M., 2009. The evaluation of various oxidants used in acid leaching of uranium. In: Hydrometallurgy Conference 2009, The South African Institute of, Mining and Metallurgy, pp. 445–456.